

Non-Contact Optical Ultrasound Concept for Biomedical Imaging

Robert Haupt¹, Charles Wynn¹, Jonathan Fincke², Shawn Zhang², Brian Anthony², Anthony Samir³, and Dennis Winston¹

¹Lincoln Laboratory, Massachusetts Institute of Technology, Lexington, MA, 02420 USA;

²Department of Mechanical Engineering, Massachusetts Institute of Technology, Cambridge, MA, 02139 USA;

³Department of Radiology, Massachusetts General Hospital, Boston, MA, 02114 USA;

DISTRIBUTION STATEMENT A. Approved for public release: distribution unlimited. This material is based upon work supported under Air Force Contract No. FA8721-05-C-0002 and/or FA8702-15-D-0001. Any opinions, findings, conclusions or recommendations expressed in this material are those of the author(s) and do not necessarily reflect the views of the U.S. Air Force. © 2016 Massachusetts Institute of Technology. Delivered to the U.S. Government with Unlimited Rights, as defined in DFARS Part 252.227-7013 or 7014 (Feb 2014). Notwithstanding any copyright notice, U.S. Government rights in this work are defined by DFARS 252.227-7013 or DFARS 252.227-7014 as detailed above. Use of this work other than as specifically authorized by the U.S. Government may violate any copyrights that exist in this work.

Formatted: Justified, Space After: 8 pt,
Line spacing: Multiple 1.08 li

Abstract

In this paper, we examine the potential of a fully noncontact-standoff laser-ultrasound concept to generate and measure elastic waves in order to construct internal structure and matrix images within biological tissue. We use a pulsed optical laser (Q-switched) as an excitation source that converts optical energy to ultrasonic waves within a tissue complex via photoacoustic (PA) mechanisms. Laser Doppler vibrometry (LDV) is then used to measure the returning signals on the tissue surface.

We report that the photoacoustic generation of elastic waves from a short optical pulse produces the compilation of elastic body and surface waves including longitudinal, shear, Rayleigh, and Love wave components. Using information from the various wave types can yield 1) tissue and bone anatomical images for medical diagnosis and 2) mechanical property distributions that have important implications in the emerging field of medical elastography.

We also examine the effects of optical excitation wavelength on the signal-to-noise ratio (SNR) and quality of ultrasonic images of the interior of tissue specimens. Optical wavelengths spanned the near infrared to the short wave infrared and included 810, 1064, 1550, and 2000 nm (all via a tunable Q-switched OPO laser). In general, but with an important exception near 1550 nm, the known tissue absorptivity implies that longer wavelength light is more strongly absorbed than shorter wavelengths. The question examined in this work is how this translates to propagating acoustic energy (ultrasonic waves) capable of penetrating several inches into tissue in order to be useful for interior imaging. We observe that wavelengths near 1550nm produce acoustic energy with the highest SNR and thus the best quality interior images while operating well within skin and eye safety standards. A simple model based on the known tissue absorptivity and photoacoustic conversion is proposed to explain these results.

Lastly, we present imaging capabilities using a non-contact laser ultrasound proof-of-concept system. Two and three dimensional time images are depth migrated and compare well with ground truth geometries, orientation, and depth of staged samples. We also generate 2D cross-sectional reflection images of a phantom limb that contains muscle and bone surrogate materials and use the data for inversion of the Young's modulus distribution in the specimen.

1. Introduction

Diagnostic ultrasound (US) is an ideal imaging modality in many respects: it is portable, low cost, has no known harmful bioeffects, and produces images with excellent spatial and temporal resolution. US can

also measure blood flow and provide information about tissue mechanical properties. Despite these advantages, MRI and CT are the dominant modalities used for many medical imaging applications including head injury, cancer, fractures and musculoskeletal disease. MRI and CT use fixed gantry-mounted systems that enable spatially reproducible images, which, permit accurate comparison of disease states over time. By contrast, US data is acquired with hand held transducers with no fixed acquisition frame. This leads to *interoperator variability* in imaged lesion geometry greatly limits current US applications. For example, the standard criteria for determining tumor progression in cancer trials do not permit tumor measurements made with US [1]. There is therefore a great need to develop systems that combine the spatial reproducibility advantages of CT and MRI with the informational, cost, portability, and low toxicity advantages of US. Such systems would enable numerous new US applications.

Using non-contact, standoff optical ultrasound has the potential to provide a fixed reference measurement capability that minimizes operator variability as experienced by contact transducer systems. Excitation and receive locations could be revisited with repeatable precision, thus enabling the capability to monitor subtle changes over time with much less error compared to the hand held transducer approach. Moreover, the appeal of conducting optical ultrasonic measurements in medical applications comes from the need in many cases to avoid contact with damaged skin, burned skin, painful regions, areas susceptible to infection and contamination, and areas awkward or difficult to reach. However, to bring such an approach into medical practice requires considerable research, development, and trial.

Non-contact optical ultrasound can be achieved via short optical pulses that generate elastic waves. The short pulse converts optical energy into mechanical energy via thermal expansion [2] causing the optical absorbing material to rapidly deform, thus launching a propagating mechanical or elastic wave response. The emerging wave can then be measured at the skin or structure surface with a LDV. Research on non-contact acoustic and vibrational ultrasound has been ongoing for the past decade [2]. Much of the research focus has been in the field of photoacoustic tomography (PAT), an emerging optical technique that is becoming increasingly popular in studies to image near surface shallow capillaries in animal tissue [2-4] with typical penetration depths less than 1 mm. The PAT technique primarily employs an optical source to cause the photoacoustic effect and contact transducers to record the response. Recent studies are exploring the LDV as a sensing device making the system totally optical [5, 6]. In these studies, measureable signals were observed to depths of < 1 cm in biological phantoms or natural tissue. However, for optical measurement systems to compete with practiced medical ultrasound, penetration depths of at least several inches are needed to probe structures of interest. Additionally, the light must be eye and skin safe for wide use in medical practice.

Optical ultrasound does not impart large-scale physical distortion or deformation due to surface loading unlike contact transducers. Contact transducers suffer problems of irreproducibility due to signal distortion based on the transducer contact pressure and coupling gel contact quality to the skin leading to operator variability. For example, the American Thyroid Association guidelines require an increase in thyroid nodule volume of more than 50%, or an increase of more than 20% in two or more measured dimensions, prior to recommending biopsy. This is because interoperator variability is so high, large increases in nodule size are necessary before nodule growth can be confidently diagnosed [3]. Another example, the European Organization for Research and Treatment of Cancer (EORTC) and Response Evaluation Criteria In Solid Tumors (RECIST) guidelines do not permit the use of ultrasound tumor measurements for the follow-up of cancer, owing to high interobserver variability. This means that patients with cancer must be followed up with CT scans (high cost and ionizing radiation) or MRI scans (high cost) [3].

In this paper, we demonstrate fully non-contact laser ultrasound in tissue and examine the effects of excitation optical wavelength, power, and spot size on ultrasonic image quality. Specifically, we examine ultrasonic image quality using optical powers within eye and skin safety limit standards. We discuss the potential of such a system to form images inside the body and discuss the advantages and drawbacks of optical laser ultrasound.

A concept noncontact laser ultrasound system is shown below in Figure 1 where, photoacoustic excitation is used in conjunction with an LDV array to acquire ultrasonic waves traveling in the body.

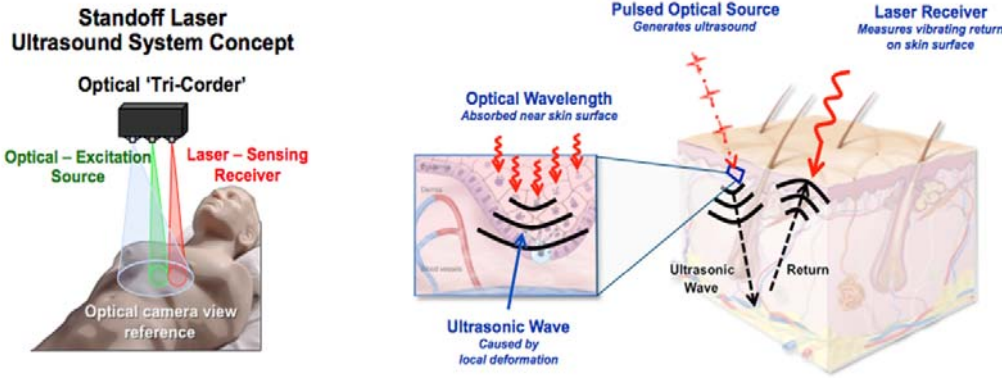


Figure 1. Notional laser ultrasound system concept to acquire elastic wave images and material properties of the body interior without contact to the subject. Pulsed light absorbs over a very short distance within the skin surface layers. The absorption creates a sudden heating, deformation, and a resultant time varying stress and strain in the skin that generates an ultrasonic wave capable of propagating into the far field within body tissue. The ultrasonic return reflected off internal structural boundaries where mechanical impedances exist is measured optically using a laser Doppler vibrometer (LDV).

2. Standoff – Noncontact Optical to Ultrasonic Wave Generation with Laser Measurement

Photoacoustic phenomena develop from photoelectrons that interact with a target surface when emitted by a very short short laser pulse (pico-nanoseconds) onto a highly optically absorptive surface of a material, such as water or biological tissue where optical energy rapidly converts into heat [1]. This heating is nearly instantaneous creating a concentration of mechanical stress within the irradiated tissue patch. The tissue is no longer in mechanical equilibrium where the stress must dissipate and generates a propagating acoustic wave into the tissue mass.

Photoacoustic phenomena and the process of acoustic and elastic wave propagation are described in detail in the literature [8, 9] from which we highlight the summary equations.

Optical Absorption Process

In the first stage of the photoacoustic process, photons are absorbed by particles comprising a tissue volume, where the absorption coefficient

$$\mu_a = \rho \sigma_a \text{ where, } \sigma_a = -4 \frac{2\pi a}{\lambda} \pi a^2 \text{Im} \left\{ \frac{n_1 - n_0}{n_1 + 2n_0} \right\} \quad (1)$$

ρ and σ_a are the particle density and cross-sectional area, a is the particle radius, where $a \ll$ the optical wavelength, and n_1 and n_0 are the refraction indices of the absorbing material and an infinite homogeneous non-absorbing medium.

For an optical pulse incident on tissue particles, the total absorbed energy, E_a becomes

$$E_a(\mathbf{r}, t) = \mu_a \int_{4\pi} I(\mathbf{r}, t, \hat{\mathbf{s}}) d\Omega = \mu_a U^{inc}(\mathbf{r}, t) \quad (2)$$

I is the specific intensity absorbed by the tissue particles at a position \mathbf{r} from light incident in a direction $\hat{\mathbf{s}}$. U^{inc} is the average incident intensity with units of J/cm^2 .

The governing relationship establishing tissue deformation and thus, acoustic or elastic wave generation evolves from the tissue temperature increase caused by the absorbed energy where

$$\rho_m C \frac{\partial T(\mathbf{r}, t)}{\partial t} - \kappa \nabla^2 T(\mathbf{r}, t) = E_a(\mathbf{r}, t) \quad (3)$$

ρ_m, C, κ, T are the tissue mass density, specific heat, thermal conductivity, and temperature, respectively. The first term in equation (3) describes the temperature increase due to optical absorption and diffusion. The optical diffusion is several orders of magnitude larger than that of the thermal diffusion, thus, the second term in equation (3) is negligible.

Optical Propagation Process

The next critical component to understanding the process of photoacoustic phenomenology is the effect of optical propagation into a scattering media such as complex biological tissues. The materials comprising tissue mass are considerably heterogeneous, where blood hemoglobin, for example, is highly absorptive to light while other tissue cells are simultaneously, highly reflective. The average incident energy can be derived showing the relationship between the incident energy density in the time domain where:

$$U^{inc}(\mathbf{r}_s, \mathbf{r}, t) = \frac{S_0}{(4\pi Dct)^{3/2}} \exp\left[\frac{|\mathbf{r}_s - \mathbf{r}|}{4Dct} - \mu_a |\mathbf{r}_s - \mathbf{r}|\right] \quad (4)$$

Optical Conversion to ultrasound wave propagation

The last critical component to describing photoacoustic conversion of light to pressure and resultant acoustic wave propagation is described next [9]. It is the acoustic or elastic wave that can be measured by an optical receiver such as a laser Doppler vibrometer or conventional contact transducer. For simplicity, we consider the case of an inviscid fluid to demonstrate the generation and propagation of the longitudinal or compressional wave from incident light.

Starting with the linear force equation,

$$\rho_m \frac{\partial^2 \mathbf{u}(\mathbf{r}, t)}{\partial t^2} = -\nabla p(\mathbf{r}, t) \quad (5)$$

where \mathbf{u} is the acoustic displacement and p is the acoustic pressure. The relationship between the heat source and the resultant pressure is shown below in terms of the optical average intensity and optical absorption coefficient:

$$\nabla^2 p(\mathbf{r}, t) - \frac{1}{v_s^2} \frac{\partial^2 p(\mathbf{r}, t)}{\partial t^2} = \frac{\beta}{c} [\mu_a + \Delta\mu_a(\mathbf{r})] \frac{\partial U(\mathbf{r}, t)}{\partial t} \quad (6)$$

The pressure distribution along the tissue column resolves to

$$p(\mathbf{r}, t) = p_0(\mathbf{r}, t) + \frac{\beta}{4\pi C} \int_V \frac{d\mathbf{r}'}{|\mathbf{r} - \mathbf{r}'|} \Delta\mu_a(\mathbf{r}') \times \left| \frac{\partial U^{inc}(\mathbf{r}', t')}{\partial t'} \right|_{t'=t-|\mathbf{r}-\mathbf{r}'|/v_s}$$

where

$$p_0(\mathbf{r}, t) = \frac{\beta\mu_a}{4\pi C} \int_V \frac{d\mathbf{r}'}{|\mathbf{r} - \mathbf{r}'|} \left| \frac{\partial U^{inc}(\mathbf{r}', t')}{\partial t'} \right|_{t'=t-|\mathbf{r}-\mathbf{r}'|/v_s} \quad (7)$$

In the above expression, $p_0(\mathbf{r}, t)$ is the incident pressure at the onset of the tissue column.

Noncontact Laser Vibrometry Sensing

A heterodyne coherent ladar design is considered for a vibrometer sensing system. In heterodyne detection, a signal of interest at some frequency is non-linearly mixed with a reference "local oscillator" (LO) that is set at a close-by frequency. The desired outcome is the difference frequency, which carries the information (amplitude, phase, and frequency modulation) of the original higher frequency signal, but is oscillating at a lower more easily processed carrier frequency. Electrical field oscillations in the optical frequency range cannot be directly measured since the relatively high optical frequencies have oscillating fields that are much faster than electronics can respond. Instead, optical photons are detected by energy or equivalently by photon counting, which are proportional to the square of the electric field and thus form a non-linear event. Thus when the LO and the signal beams impinge together on a target surface they "mix", producing heterodyne beat frequencies.

The performance of a laser vibrometer is determined by its noise floor and is described in []. The noise floor consists of 1) shot noise that dominates the noise floor at ultrasonic frequencies, 2) speckle noise that mainly contributes noise in the audible acoustic band, and 3) platform and subject target vibration caused by motion by a variety of potential sources other than the intended system optical excitation source.

Shot noise arises from statistical fluctuations in measurements. The detected electrical current for a heterodyne ladar is

$$i(t) = i_{LO} + i_s(t) + 2\sqrt{\eta_h i_{LO} i_s(t)} \cos[\omega_{IF} t + \theta(t)] \quad (8)$$

where i_{LO} and $i_s(t)$ are the currents from the local oscillator and signal, η_h is the heterodyne mixing efficiency (0 to 1), ω_{IF} is the intermediate frequency (carrier signal is mixed with the local oscillator to produce a difference or beat frequency to improve signal gain), and $\theta(t)$ is the phase shift. ω_{IF} is equal to the acousto-optic modulator frequency offset plus the Doppler offset due to platform motion. The phase shift is given by

$$\theta(t) = 2kx(t) + \theta_s(t) = \frac{4\pi x(t)}{\lambda} + \theta_s(t) \quad (9)$$

where $x(t)$ is the line-of-sight distance between the ladar and tissue surface, $\theta_s(t)$ is the random phase of the speckle lobe, and λ is the optical wavelength of the vibrometer. $x(t)$ changes due to body vibrations and movement, laser platform vibration and pointing jitter.

A critical design parameter of the laser vibrometer vibration sensing system is the carrier-to-noise ratio (CNR). Specifically, the received number of photoelectrons per second, ϕ_e (optical return from the vibrating tissue surface) over the vibrometer demodulated bandwidth determines the received signal quality. The greater the number is of photoelectrons received by the laser sensing system, the lower the shot noise is, thus, resulting in a more sensitive vibrometer. The CNR can be increased by simply increasing the sensing system power and by decreasing the laser beam diameter that impinges upon the tissue surface. However, when using too much power, and too small a beam diameter, the risk of skin and eye damage can occur, and prompts design level constraints to operate within safety limits. The shot noise spectrum of the surface particle velocity, $A_{v,sh}$ as a function of frequency, f , is proportional to received returning photoelectrons such that

$$A_{v,sh}(f) = \frac{f\lambda}{\sqrt{\phi_e}} \quad (10)$$

Another important noise source is that from speckle. Speckle is the noise that occurs due to the distribution of optical scatters on the tissue surface encountered by a laser beam. For a diffuse surface,

there are likely many scatterers (based on surface roughness) that *reflect* light back to the receiver. The speckle noise contribution to the laser sensing system can be reduced by signal time integration with respect to the same realization of scatterers. Increasing the integration time reduces speckle noise and thus improves the system sensitivity. However, if during the allotted integration summing time, the beam changes position on the target due to platform motion, beam jitter, or target movement, the speckle realization changes, creating translation or dynamic speckle and the noise floor increases. Faster beam translation speeds across the tissue sample increase the speckle noise floor contribution even more. The speckle noise amplitude

$$A_{v,sp}(f) = \lambda \sqrt{\frac{\pi f_{exc}^2}{12}} \sqrt{\frac{2\alpha}{\alpha^2 + (2\pi f)^2}} \quad (11)$$

where $\alpha = 2\pi f_{exc}$ and $f_{exc} = v_t/d$ (beam translation velocity on target over the beam diameter) is the exchange rate of the speckle pattern.

In terms of laser vibrometer performance for ultrasonic measurements, the shot noise contribution (at 1 MHz) is anticipated to dominate the noise floor sensitivity. However, when introducing system motion, speckle noise becomes a significant factor. Even, subtle motion, with a small laser beam diameter (on the order of millimeters) can produce significant fluctuations in the speckle realization and resultant noise floor.

3. Standoff – Noncontact Laser Ultrasound (N-CLUS) Measurement System

A proof-of-concept system was constructed to 1) explore the phenomenology that control optical absorption and ultrasonic wave generation, 2) explore the variety and compilation suite of elastic/ultrasonic waves that are generated from a photoacoustic source, 3) explore data acquisition configurations that yield anatomical images of biological tissue interior, 4) examine and compare anatomical image quality as a function of the optical excitation wavelength.

The optical excitation source is driven by a Continuum Panther OPO or a Continuum Minilite YAG Q-switched laser. A fast steering mirror is used to position the laser beam onto the sample surface within submillimeter increments in x and y translation. A commercial Polytec, OFV 5000 LDV or the custom MIT Lincoln Lab biomedical LDV beam can be positioned to the receiving location. The Polytec requires a dusting of fine reflexite beads on the receiving point to achieve an acceptable noise floor to observe the ultrasonic signal return in response to photoacoustic excitation. Commercially available Olympus 1 MHz transducers are used as a contact receiver to measure the ultrasonic returns from the photoacoustically driven ultrasonic waves traveling in the tissue samples to provide ground truth signal levels.

Return ultrasonic time series are collected on a Tektronix 200 MHz digitizing scope and then recorded on a laptop computer. The excitation beam location is controlled by the fast steering mirror positioned an automated computer routine in LabView software. Typically, transverse scan lines are steered across the sample. A compilation of scan lines can then be used to form a 3D time image that can be processed and converted to depth. A single scan line can be used to form a 2D cross-sectional profile in the tissue specimen. The 2D scan line is referred to an off end shot record, where the receiver station is at the near end of the cross-section and the excitation source is moved incrementally away from the receiver in a bistatic geometry.

The increasing bistatic source and receiver geometry was used to accommodate standard seismic data processing algorithms to remove the effects of time distortion such as, normal moveout (NMO) and diffraction of point scatterers. NMO corrections and migration are used to reduce the plotted cross-sectional data to obtain depth images of the tissue specimen interior. The experimental measurement configuration is shown in figure 4 along with an example off end shot record from a phantom bone material slab.

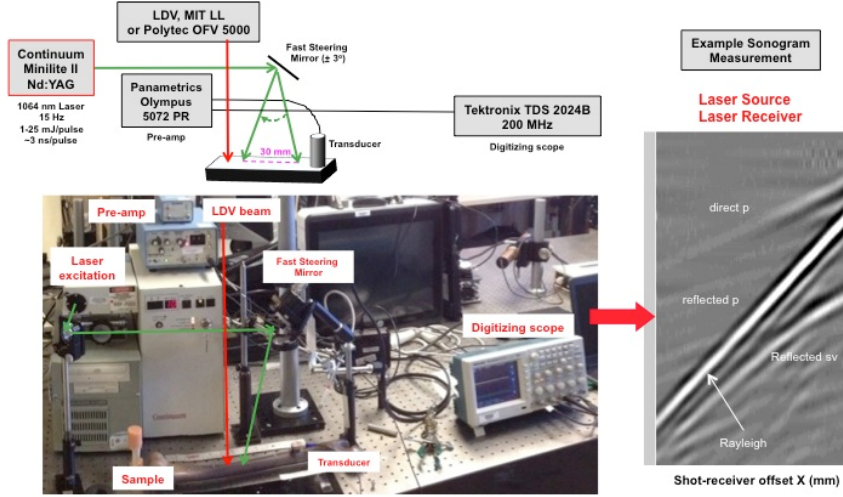


Figure 4. Non-contact Laser Ultrasound experimental system using commercial available components. The LDV receive system is a Polytec OFV 5000. To the far right, an example sonogram time series off-end shot record is shown exhibiting the variety of resultant ultrasonic/elastic waves observed from the phantom slab.

4. Standoff – Noncontact Measurement of Ultrasonic Wave Types

We observe that a narrow optical beam can photoacoustically generate the full suite of elastic/ultrasonic waves in rigid biological tissue such as bone that are well described in the seismological literature [1] while compressional waves dominate in biomass tissue such as muscle, skin, and fat. Elastic wave types and phenomena generated from the photoacoustic source in our experiments are measured using oriented contact transducers and a non-contact nadir viewing LDV. For the off-end shot record, we refer to the nadir view as the vertical particle velocity component. The horizontal view along the scan line is referred to as the inline horizontal particle velocity and the horizontal crossline particle velocity motion is measured ninety degrees to the inline direction.

The elastic wave propagation in a simple 2D bone phantom slab is shown in figure 5. For this example, the LDV and contact transducer are used to compare the observed wave type measurements. The LDV measures the vertical motion where the contact transducer measures the inline horizontal component. The wave types are inferred from the analysis of the measured wave speeds and return geometries observed from the sample. Simple analysis shows that compressional (body), shear (body), and Rayleigh (surface) waves are present for direct and reflected transmissions. Direct wave transmissions are depicted by linear sloping events that ‘fall’ away from the near trace. The steeper the slope, the slower the wave velocity is. Reflected waves exhibit a hyperbolic moveout that is proportional to the bistatic excitation source and receiver spacing. Hyperbolic moveout is described by the following expression and can be applied to correct the time distortion to produce a depth-converted image [2].

$$\Delta t \approx \frac{x^2}{2t_0 V^2} \left\{ 1 - \left(\frac{x}{4h} \right)^2 \right\} \quad (1)$$

where the time correction, Δt is related to the horizontal receiver offset, x , zero-offset travel time, t_0 , elastic wave speed in the media, V , and the normal depth to the reflector, h . Equation (1) can be applied to remove the curved time distortion to restore the shape of a flat reflector at depth.

In figure 5, the ultrasonic / elastic wave type is inferred from wave speed analysis. A variety of direct and reflected waves are observed including, compressional (longitudinal), shear, and Rayleigh components. In the shot records shown in figure 5a, we observe direct, reflected, and multiple reflection p-wave events. Shear vertical, Rayleigh, and Lamb waves are also observed. In figure 5b, shot records from non-contact excitation and measurement exhibit a variety elastic waves that are inferred from wave speed analysis. Acoustic, longitudinal, shear, and Rayleigh waves are present and are consistent with direct transmission measurements using Olympus longitudinal and shear transducers.

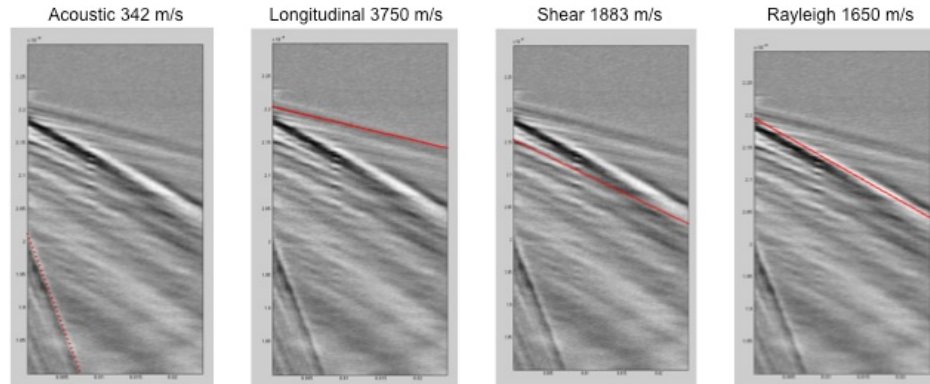


Figure 5a. Elastic wave components observed from photoacoustic excitation in cow tibia bone sample. Elastic wave types are determined by travel speed analysis.

Next, we examined the elastic wave generation from a point photoacoustic source as a function of receiver orientation. Orientations include: 1) shear cross-line, where the particle velocity is measured in the horizontal y direction ninety degrees to the direction of propagation, 2) shear inline, where the particle velocity is measured in the horizontal x direction and in the direction of propagation, and 3) vertical z direction.

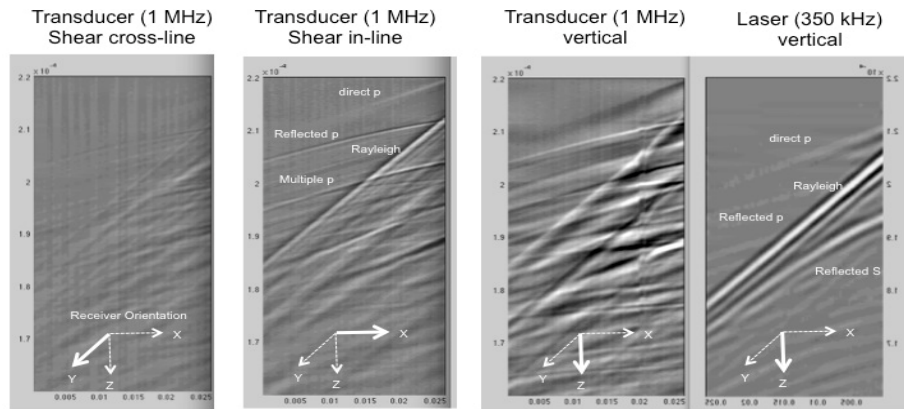


Figure 5b. Elastic wave components observed from photoacoustic excitation bone phantom slab. All the receivers measure the set of elastic waves, however, the wave amplitudes vary significantly depending on receiver orientation. The cross-line shear receiver shows the smallest amplitudes since the majority of the energy is transmitted 90 degrees to the propagation direction. The inline shear

measurements exhibit strong high frequency content with some interference between wave types. The inline SNR amplitude is strong since the bistatic source receiver spacing is typically larger than the depth of the bone phantom-table reflector. The vertical component displays a strong SNR with several multiple reflections and interference as would be expected for the measurement geometry.

5. Effects of Optical Wavelength on Image Quality and Patient Safety

We examine the effects of the optical excitation wavelength on SNR and image quality while holding the spot size constant at 1.6mm. These effects are shown for four common optical wavelengths listed in figure 6. Figure 3 predicts that longer optical wavelengths absorb in shorter distance in the steak surface resulting in more power and higher frequency content.

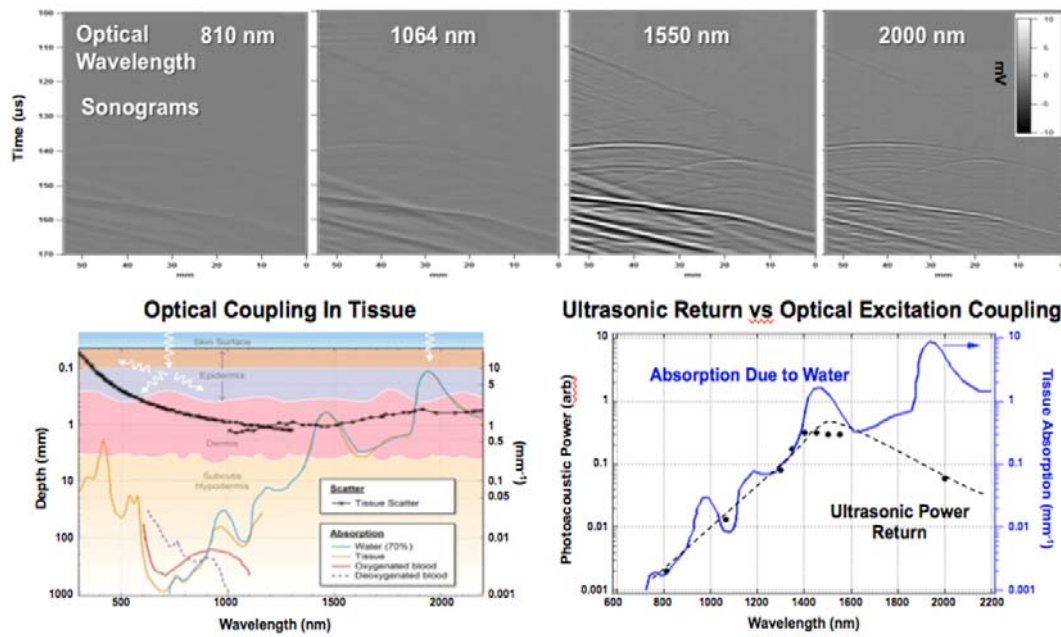


Figure 6. Effects of optical excitation plotted for four wavelengths while maintaining a constant spot size and power per square area. Sonogram time series 2D images are presented relative to the maximum amplitude between the four images.

1550nm and 2000nm optical wavelengths produce strong signatures and good SNR while maintaining eye and skin safety. It appears that the 1550nm wavelength yields the best ultrasonic SNR with clear diffraction signatures from the two embedded rods and the reflection from the table. The 2000nm wavelength also shows very strong signatures with a slightly higher frequency content compared to the 1550nm image. Moreover, since the 2000nm image has higher ultrasonic frequency content, the higher frequencies tend to attenuate more rapidly with depth and yield a slightly lower SNR. Thus, it appears that the 1550nm data may yield the best overall image quality of the four wavelength examples.

6. N-CLUS Imaging in Biological Tissue

In this section, we examine the capability of the N-CLUS system to generate ultrasonic images in common biological tissue in two and three dimensions. Specifically, we explore the potential of the system to detect and image foreign materials and wounds in a tissue mass.

Time series sonogram images are formed in 2D where the horizontal x-axis represents the optical source and receiver offset in range while the vertical z-axis represents two-way travel time or depth into the sample. In figure 11, 2D sonograms are displayed for three different conditions: 1) clear steak slab, 2) single metal 1 mm rod embedded in the steak slab, and 3) the wound left behind from the rod removed. Each condition is shown using the LDV in nadir view and an inline horizontal contact transducer as receivers. Metal sliver and wound both show strong signatures using the N-CLUS system. The undisturbed beef sample shows the direct compressional surface wave event in early times and the hyperbolic table reflection event in later times.

When the 1 mm rod is embedded in the beef, a diffraction pattern is measured along the x-axis and is visible in both the LDV and contact transducer receiver images. When the 1 mm rod is removed, the exit wound exhibits a strong diffractive pattern. In this condition, the wound gap, although mostly closed, exhibits a large impedance due to the interface of the wound air volume and beef tissue.

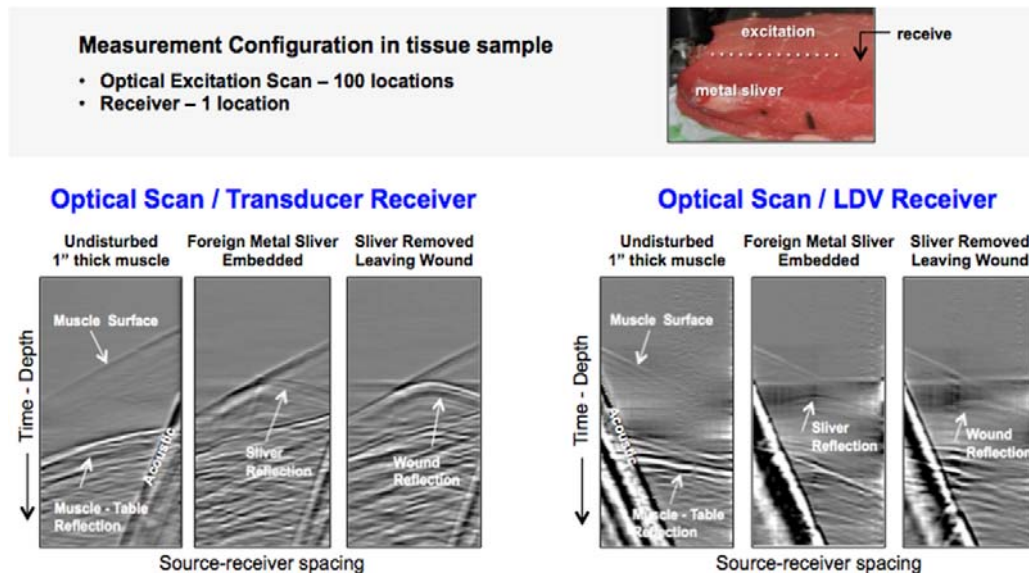


Figure 7. 2D Sonogram Images of embedded metal sliver and wounds in steak sample. Left panel shows the nadir view LDV and inline contact transducer receiver time images of undisturbed beef tissue. The center panel shows the corresponding images containing a 1 mm metal rod embedded in the beef. The right panel show the exit wound in beef by the removal of the 1 mm rod.

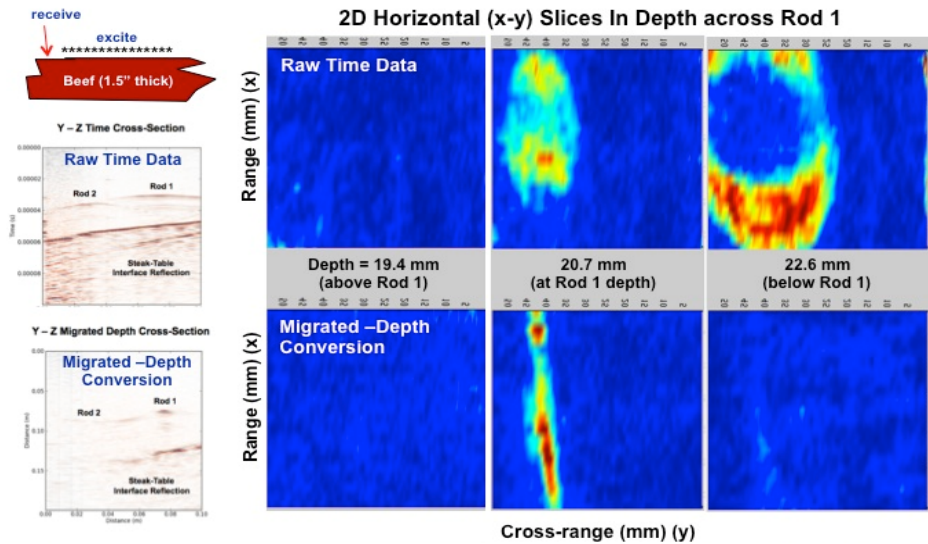


Figure 8. 2D Sonogram and 3D Depth Migrated Images of embedded rods in steak sample. Migration algorithm reduces time distortion and image spreading due to diffraction scattering.

In figure 8, we produce a 3D image of the two 1 mm rods embedded in the beef tissue. Two plots are shown for the unmigrated- time sonogram and migrated-depth images. First, reviewing the time sonogram in the upper three panels, at the time of interception of the upper rod, a broad image is observed in the x-y image plane that registers a significant portion of the diffraction response coming from the rod itself. At a later time corresponding to a larger depth, the diffraction response shows itself over a greater region as the traveling wave increases with distance from the rod. In reality, if one were to place a pin at the site of the time image, the rod would not be encountered since the diffraction is a time distortion product.

The bottom three panels show the images from the depth-migrated processed data. *Seismic migration* is a process to "migrate" the recorded events to their correct spatial positions by backward projection or depropagation based on wave theoretical considerations. Diffractions are reduced to the scattering source using a Kirchhoff migration scheme []. The bottom figure panels show the diffraction pattern is collapsed to its origin point at its approximate depth inside the steak sample. In the x,y depth slice below, there is no evidence of the rod in the image, unlike the time sonogram.

2D Laser Ultrasound Imaging Around Phantom Bone/Muscle Complex

In the previous sections, we demonstrated that it is possible to acquire ultrasonic reflection images of high-contrast foreign objects imbedded in tissue mass using a non-contact laser ultrasound approach. In this section, we explore the potential to form a 2D reflection image encompassing a bone/muscle complex phantom. In these measurements, the phantom specimen rests on a rotational stage, where a contact piezoelectric Olympus transducer is fixed to a single location. As the stage rotates, the transducer also rotates and acts as a receiver to a photoacoustic source aimed at a fixed orientation. In this configuration, the optical source beam and receiver change relative raypaths since the excitation beam encounters a different location on the target phantom when it rotates. This configuration is shown in the figure below.

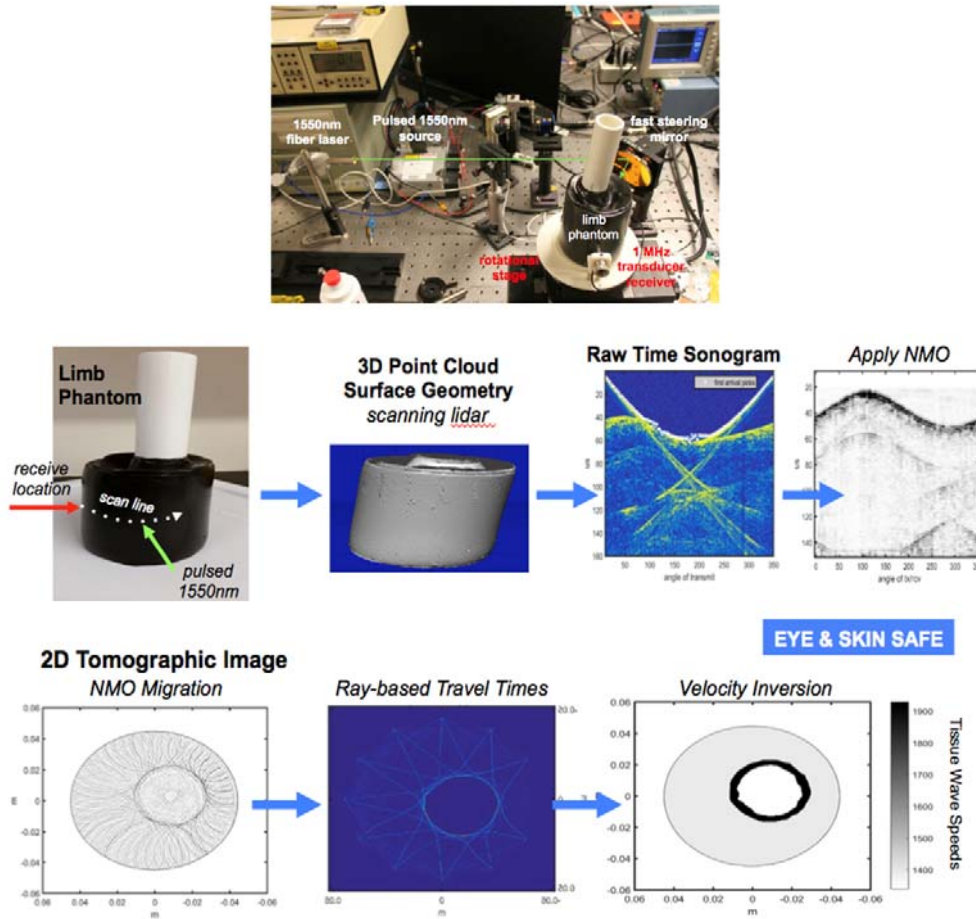


Figure 9. 2D Slice of rotational reflection laser ultrasound image of phantom limb with PVC pipe as bone surrounded by gel as muscle mass. In this example, a pulsed 1550nm laser excites the ultrasonic wave from standoff while a piezoelectric contact transducer acts a receiver measuring the return signal.

Next, we repeat the rotational stage measurements, but now replace the contact piezoelectric transducer with a non-contact laser vibrometer receiver representing the N-CLUS system. In these measurements, a Polytec OFV5000 is used as the receiver and is placed 1 meter from the phantom sample. Reflexite dust is applied on the phantom sample surface to enhance the performance of the vibrometer noise floor and is required to achieve adequate SNR to observe the ultrasonic signal generated by the photoacoustic source (1550nm wavelength). The Polytec employs a 632nm wavelength at 2mV and is skin and eye safe at this power level. We then compare the signal quality and SNR achieved for different transmit and receive scenarios using 1) transducers only in a water tank, 2) a hybrid of optical excitation and transducer receiving, and 3) a total non-contact optical transmit and receive configuration (N-CLUS).

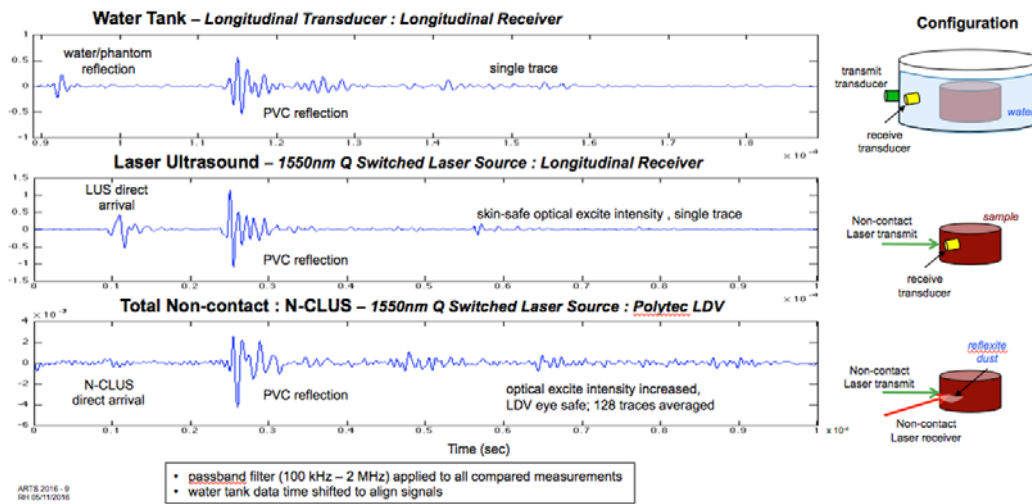


Figure 10. Comparison of time series traces measured by state-of-the-art piezoelectric transducers in a water tank, laser photoacoustic excitation measured by a contact transducer, and total non-contact laser ultrasound.

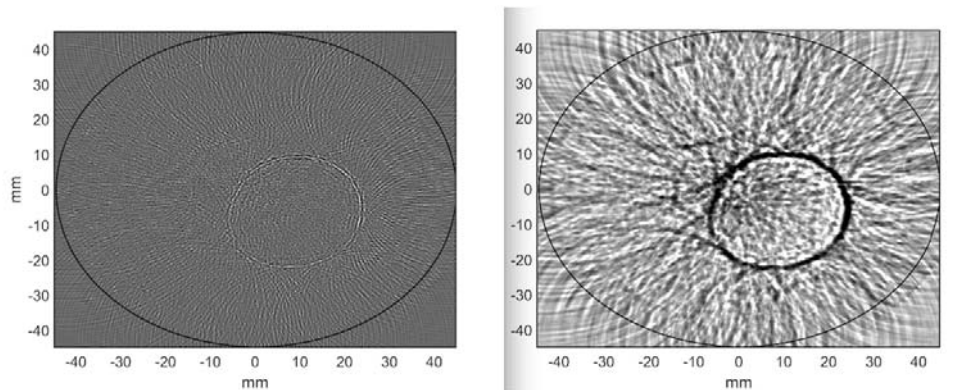


Figure 11. 2D Slice of rotational reflection laser ultrasound image of phantom limb with PVC pipe as bone surrounded by gel as muscle mass. In this example, a pulsed 1550nm laser excites the ultrasonic wave from standoff while a non-contact Polytec OFV5000 acts a receiver measuring the return signal from a nadir orientation.

In figure 10, we analyze the signal quality of state-of-the-art ultrasonic waves propagating in the phantom limb specimen. A water tank apparatus was developed by MIT MEDRC to acquire ultrasonic imagery for residual limbs for amputees. The ultrasound system consist of focused 5 MHz transducers that transmit and receive ultrasonic waves that can be acquired in bi-static arrangements for reflection or tomographic data. The water tank data are compared with the optical excitation source using a 1 MHz contact transducer receiver, and a totally optical arrangement using a total non-contact optical excitation and laser Doppler vibrometer receiver.

The optical excitation and ultrasound excitation compare very closely in SNR and signal quality as measured by a remote contact transducer for a single excitation pulse. The total non-contact arrangement compares closely as well, however, the SNR is slightly degraded compared to the other two cases. More importantly, the non-contact arrangement can be achieved in a reasonable time frame while producing a strong signal. Lastly, the non-contact optical ultrasound images shown in figure 10, clearly show the bone phantom embedded in the muscle tissue and compare very closely with the image quality and feature definition observed in the optical excitation, transducer measurement arrangement.

7. Discussion and Conclusions

In this paper, we examine the potential of a fully noncontact-standoff laser-ultrasound concept to generate and measure elastic waves in order to construct internal structure and matrix images within biological tissue. We use a pulsed optical source (Q-switched laser) that converts optical energy to ultrasonic waves within a tissue complex via photoacoustic (PA) mechanisms. Laser Doppler vibrometry (LDV) and contact ultrasonic transducers are used to measure the returning signals on the tissue surface.

We report that the photoacoustic generation of elastic waves from a short optical pulse produces the compilation of elastic waves including longitudinal, shear, and surface wave components. Using information from the various wave types can yield tissue and bone anatomical images for medical diagnosis and mechanical property distributions that can have important implications in the emerging field of medical elastography. Moreover, shear wave properties may yield important information pertaining to changing biological conditions in the body.

We also examine the effects of optical excitation wavelength, spot size, and power on the SNR and quality of ultrasonic images of the interior of tissue specimens. Optical wavelengths examined are 810, 1064, 1550, and 2000 nm that are emitted from a tunable Q-switched OPO laser. Results show that longer wavelength excitation is absorbed over a shorter distance than shorter wavelengths and produces reasonable SNR ultrasonic waves that are capable of traveling several inches into tissue. We observe that wavelengths of 1550nm and 2000nm produce the highest SNR signals and best quality interior images while operating well within skin and eye safety standards. Two and three dimensional time images are depth migrated and compare well with ground truth geometries, orientation, and depth of staged samples. Results indicate that a standoff noncontact laser ultrasound system may be useful for creating images of the body's interior and has potential to operate within skin and eye safety standards.

8. Advantages and disadvantages of optical laser ultrasound compared to contact transducers

Ideally, if optical laser ultrasound produced a comparable or better signal quality to conventional contact ultrasound systems, then the optical approach would likely be the method of choice. The optical image acquisition approach has a number of significant advantages over contact transducer measurements. Optical advantages include: 1) spatial sampling can approach submillimeter resolution using coherent multipixel arrays, 2) measurements can access injured body regions, surfaces, skin conditions, open wounds or regions during surgery, difficult and awkward to reach regions, 3) no physical pressure of the device applied to the skin or body, 4) reduced injury to operators due to device pressure applications to patients, 5) no need or contamination from coupling gels (as in the case of contact ultrasound devices), and 6) no SNR variability due to applied hand pressure as in the case of contact transducers.

In our studies [], we attempted to identify the limitations of optical ultrasound. Our measurements show that the achievable SNR from contact ultrasound is likely to be better than that of laser sensing. However, the gain observed from contact methods are partially due to application of coupling gels and pressure force to improve the signal. Without these components, conventional contact ultrasound signal quality and SNR degrades dramatically. Improving the SNR for laser vibrometry measurement on skin or biological tissue as obtained using the custom vibrometer introduced in this paper is likely to be challenging. Laser power can be increased to produce lower shot noise. We anticipate that data processing methods can be improved in our current system to increase the vibrometer sensitivity. In

addition, balance detectors can be optimized to maximize signal gain without saturating and in turn degrading the noise floor performance.

Speckle noise due to subtle and involuntary body movements, laser beam jitter, and platform (laser mount) movement all contribute to an increase in the vibrometer noise floor reducing its sensitivity. In many cases, these effects can be very significant making signal detection difficult and inconsistent. Beam tracking on a specific skin location may help to mitigate or reduce these sources of noise.

Limitations in photoacoustic excitation also present disadvantages for an optical source. Choosing the proper optical frequency is critical for generating a coherent signal. Ideally, the optical wavelength that absorbs very rapidly while minimizing diffusion into the skin is optimal for maximum energy conversion from light to heat. Q-switched lasers can provide ample and useful power to generate elastic waves in biological tissue. However, using wavelengths at approximately 250-300 nm may be considered dangerous to the resonance behavior of DNA. Using too high a power can also cause skin burning.

However, results from our studies show that there is a plausible route that exists for standoff laser ultrasound. Specifically, using longer wavelength optical excitation in the range of 1500-2000nm can potentially offer a skin and eye safe excitation system for use in medical practice. Laser acquisition and sensing arrays and can be engineered to provide reasonable data collection times and scan areas competitive with existing contact ultrasound systems. If in the event, laser vibrometry becomes the limiting factor to the success of non-contact laser ultrasound, a hybrid system consisting of optical excitation (PA) and a contact transducer can still offer a very significant capability. The hybrid combination can provide a fixed reference system approach that will greatly reduce operator variability as observed with conventional hand held transducer systems. In addition, the hybrid or total non-contact laser system is likely to yield image quality and resolution that are competitive with MRI and CT, but, at a much lower cost, portable capability, and free of significant hazards.

7. References

1. W. Hendee and E. Ritenour, Medical Imaging Physics, Fourth Edition, ISBN: 0-471-38226-4 2002 Wiley-Liss, Inc.
2. Wang LV. Tutorial on photoacoustic microscopy and computed tomography. IEEE Journal of Selected Topics in Quantum Electronics. 2008;14(1):171–179.
3. C. Li and L. V. Wang, Photoacoustic tomography and sensing in biomedicine, Physics in medicine and biology 54, R59–97 (2009).
4. Yin, B., D. Xing, Y. Wang, Y. Zeng, Y. Tan, and Q. Chen, Fast photoacoustic imaging system based on 320-element linear transducer array, Physics in Medicine and Biology 49, 1339–1346 (2004).
5. Xu, G., C. Wang, T. Feng, D. Oliver, and X. Wang, Non-contact photoacoustic tomography with a laser Doppler vibrometer, Proc. SPIE Vol. 8943 89332 7 pgs., 2014.
6. Rousseau, G., A. Blouin, and J. Monchalain, Non-contact photoacoustic tomography and ultrasonography for tissue imaging, Biomedical Optics Express, Vol. 3, No. 1, pgs. 16-25, Jan, 2012.
7. Haupt, R. and L. Jiang, Ultrasonic Shear-wave Imaging for Biomedical Diagnostics, 2014.
8. Ripoll, J. and V. Ntziachristos, Quantitative point source photoacoustic inversion formulas for scattering and absorbing media, Physical Review E 71. 031912, (2005).
9. Schurig, D.A., G. Klunder, M. Shannon, R. Russo, and R. Silva, Signal analysis of transients in pulsed photoacoustic spectroscopy, Rev. Sci. Instrum. 64(2), Feb, 1993.
10. Jiang, L.A., M. Alota, R. Haupt, J. Chen, and R. Marino, Laser vibrometry from a moving ground vehicle, Applied Optics, Vol. 50, No. 15, 2011.
11. Muscle velocity
12. SNR vs axial load
13. Allen, T., B. Cox, and P. Beard, Generating photoacoustic signals using high-peak power pulsed laser diodes, Proc. SPIE Vol. 5696, pp 233-242, Jan, 2005.

14. Maslov, K. and L. Wang, Photoacoustic imaging of biological tissue with intensity-modulated continuous-wave laser, *Journal of Biomedical Optics* 13(2), 024006 5 pgs., Apr, 2008.
15. ANSI Z136.1—2007; American National Standard for Safe Use of Lasers, Laser Institute of America (Orlando, FL; 2007).
16. M. Xu and L. Wang, “Photoacoustic imaging in biomedicine”, *Rev. Sci. Inst.* 77, 041101 (2006).
17. [REFGusev] **“Laser Optoacoustics” Gusev and Karabutov; Berthelot and Busch-Vishniac, J. Acoust. Soc. Am. 81, 317 (1987); Lyamshev, Sov. Phys. Acoust. 27, 4 (1981)**